



Optical NP problem solver on laser-written waveguide platform

MARÍA RAMOS VÁZQUEZ,^{1,2} VIBHAV BHARADWAJ,^{3,4} BELÉN SOTILLO,³
SHU-ZEE A. LO,⁵ ROBERTA RAMPONI,³ NIKOLAY I. ZHELUDEV,^{2,6}
GUGLIELMO LANZANI,⁴ SHANE M. EATON,³ AND CESARE SOCI^{2,5,*}

¹ICRM, Interdisciplinary Graduate School, Nanyang Technological University, Singapore

²Centre for Disruptive Photonic Technologies, TPI, Nanyang Technological University, Singapore

³IFN-CNR, Department of Physics, Politecnico di Milano, Milano, Italy

⁴Center for Nano Science and Technology, Istituto Italiano di Tecnologia, Milano, Italy

⁵Division of Physics and Applied Physics, SPMS, Nanyang Technological University, Singapore

⁶Optoelectronics Research Centre & Centre for Photonic Metamaterials, University of Southampton, UK

*csoci@ntu.edu.sg

Abstract: Cognitive photonic networks are researched to efficiently solve computationally hard problems. Flexible fabrication techniques for the implementation of such networks into compact and scalable chips are desirable for the study of new optical computing schemes and algorithm optimization. Here we demonstrate a femtosecond laser-written optical oracle based on cascaded directional couplers in glass, for the solution of the Hamiltonian path problem. By interrogating the integrated photonic chip with ultrashort laser pulses, we were able to distinguish the different paths traveled by light pulses, and thus infer the existence or the absence of the Hamiltonian path in the network by using an optical correlator. This work proves that graph theory problems may be easily implemented in integrated photonic networks, down scaling the net size and speeding up execution times.

© 2018 Optical Society of America under the terms of the [OSA Open Access Publishing Agreement](#)

OCIS codes: (160.2750) Glass and other amorphous materials; (200.4960) Parallel processing; (230.7370) Waveguides; (320.2250) Femtosecond phenomena; (350.3390) Laser materials processing.

References and links

1. P. E. Dunne, "An annotated list of selected NP-complete problems," http://cgi.csc.liv.ac.uk/~ped/teachadmin/COMP202/annotated_np.html.
2. F. Harary and I. C. Ross, "A procedure for clique detection using the group matrix," *Sociometry* **20**, 205–215 (1957).
3. S. Dolev and H. Fitoussi, "Masking traveling beams: Optical solutions for NP-complete problems, trading space for time," *Theor. Comput. Sci.* **411**, 837–853 (2010).
4. L. Fortnow, *The golden ticket: P, NP, and the search for the impossible* (Princeton University Press, 2013).
5. S. Aaronson, "NP-Complete Problems and Physical Reality," *ACM Sigact News* **36**, 30–52 (2005).
6. D. T. Chiu, E. Pezzoli, H. Wu, A. D. Stroock, and G. M. Whitesides, "Using three-dimensional microfluidic networks for solving computationally hard problems," *Proc. Natl. Acad. Sci. U.S.A.* **98**(6), 2961–2966 (2001).
7. R. H. Lathrop, "The protein threading problem with sequence amino acid interaction preferences is NP-complete," *Protein Eng.* **7**(9), 1059–1068 (1994).
8. C. Guyeux, N. M. Côté, J. M. Bahi, and W. Bienia, "Is protein folding problem really a NP-complete one? First investigations," *J. Bioinform. Comput. Biol.* **12**(1), 1350017 (2014).
9. K. A. Dill, S. B. Ozkan, M. S. Shell, and T. R. Weikel, "The protein folding problem," *Annu. Rev. Biophys.* **37**, 289–316 (2008).
10. A. S. Fraenkel, "Complexity of protein folding," *Bull. Math. Biol.* **55**(6), 1199–1210 (1993).
11. A. M. Childs, D. Gosset, and Z. Webb, "Universal computation by multiparticle quantum walk," *Science* **339**(6121), 791–794 (2013).
12. J. L. O'Brien, "Optical quantum computing," *Science* **318**(5856), 1567–1570 (2007).
13. J. B. Spring, B. J. Metcalf, P. C. Humphreys, W. S. Kolthammer, X. M. Jin, M. Barbieri, A. Datta, N. Thomas-Peter, N. K. Langford, D. Kundys, J. C. Gates, B. J. Smith, P. G. R. Smith, and I. A. Walmsley, "Boson sampling on a photonic chip," *Science* **339**(6121), 798–801 (2013).
14. N. Spagnolo, C. Vitelli, M. Bentivegna, D. J. Brod, A. Crespi, F. Flamini, S. Giacomini, G. Milani, R. Ramponi, P. Mataloni, R. Osellame, E. F. Galvao, and F. Sciarrino, "Experimental validation of photonic boson sampling," *Nat. Photonics* **8**, 615–620 (2014).

15. G. D. Marshall, A. Politi, J. C. Matthews, P. Dekker, M. Ams, M. J. Withford, and J. L. O'Brien, "Laser written waveguide photonic quantum circuits," *Opt. Express* **17**(15), 12546–12554 (2009).
16. Q. Liu, L. Wang, A. G. Frutos, A. E. Condon, R. M. Corn, and L. M. Smith, "DNA computing on surfaces," *Nature* **403**(6766), 175–179 (2000).
17. Q. Ouyang, P. D. Kaplan, S. Liu, and A. Libchaber, "DNA solution of the maximal clique problem," *Science* **278**(5337), 446–449 (1997).
18. K. W. Huang, J. L. Chen, C. S. Yang, and C. W. Tsai, "A memetic particle swarm optimization algorithm for solving the DNA fragment assembly problem," *Neural Comput. Appl.* **26**, 495–506 (2015).
19. H. Wu, "An improved surface-based method for DNA computation," *Biosystems* **59**(1), 1–5 (2001).
20. T. Haist and W. Osten, "An optical solution for the traveling salesman problem," *Opt. Express* **15**(16), 10473–10482 (2007).
21. M. Oltean and O. Muntean, "Evolutionary design of graph-based structures for optical computing," in *International Workshop on Optical Supercomputing*, (Springer Berlin Heidelberg, 2009), pp. 56–69.
22. K. Wu, J. García de Abajo, C. Soci, P. P. Shum, and N. I. Zheludev, "An optical fiber network oracle for NP-complete problems," *Light Sci. Appl.* **3**, e147 (2014).
23. M. Oltean, "Solving the Hamiltonian path problem with a light-based computer," *Nat. Comput.* **7**, 57–70 (2008).
24. W. Hu, K. Wu, P. P. Shum, N. I. Zheludev, and C. Soci, "All-Optical Implementation of the Ant Colony Optimization Algorithm," *Sci. Rep.* **6**, 26283 (2016).
25. K. Wu, C. Soci, P. P. Shum, and N. I. Zheludev, "Computing matrix inversion with optical networks," *Opt. Express* **22**(1), 295–304 (2014).
26. B. Gholipour, P. Bastock, C. Craig, K. Khan, D. Hewak, and C. Soci, "Amorphous Metal-Sulphide Microfibers Enable Photonic Synapses for Brain-Like Computing," *Adv. Opt. Mater.* **3**, 635–641 (2015).
27. N. M. Estakhri, B. E. Edwards, and N. Engheta, "Solving Integral Equations with optical Metamaterial-Waveguide Networks" in *Conference on Lasers and Electro-Optics*, OSA Technical Digest (Optical Society of America, 2017), paper FTh1G.2.
28. Y. Shen, N. C. Harris, S. Skirlo, M. Prabhu, T. Baehr-Jones, M. Hochberg, X. Sun, S. Zhao, H. Larochelle, D. Englund, and M. Soljačić, "Deep learning with coherent nanophotonic circuits," *Nat. Photonics* **11**, 441–446 (2017).
29. R. W. Boyd, J. E. Heebner, N. N. Lepeshkin, Q. H. Park, A. Schweinsberg, G. W. Wicks, and R. M. Boysel, "Nanofabrication of optical structures and devices for photonics and biophotonics," *J. Mod. Opt.* **50**, 2543–2550 (2003).
30. K. Yamada, T. Tsuchizawa, R. Kou, H. Nishi, H. Shinjima, Y. Ishikawa, K. Wada, and S. Mutoh, "Silicon photonic platform for telecommunications applications," in *Photonics Conference* (IEEE, 2011), pp. 591–592.
31. Y. Yang, Y. Ma, H. Guan, Y. Liu, S. Danziger, S. Ocheltree, K. Bergman, T. Baehr-Jones, and M. Hochberg, "Phase coherence length in silicon photonic platform," *Opt. Express* **23**(13), 16890–16902 (2015).
32. P. Frisco, C. Henkel, and S. Tengely, "An algorithm for SAT without an extraction phase," in *International Workshop on DNA-Based Computers* (Springer, 2005), pp. 67–80.
33. N. Spagnolo, L. Aparo, C. Vitelli, A. Crespi, R. Ramponi, R. Osellame, P. Mataloni, and F. Sciarrino, "Quantum interferometry with three-dimensional geometry," *Sci. Rep.* **2**, 862 (2012).
34. Corning, "Corning EAGLE2000 AMLCD glass substrates material information," <http://www.corning.com/displaytechnologies>.
35. T. Meany, S. Gross, N. Jovanic, A. Arriola, M. J. Steel, and M. J. Withford, "Towards low-loss lightwave circuits for non-classical optics at 800 and 1,550 nm," *Appl. Phys., A Mater. Sci. Process.* **114**(1), 113–118 (2014).
36. L. Sansoni, F. Sciarrino, G. Vallone, P. Mataloni, A. Crespi, R. Ramponi, and R. Osellame, "Polarization entangled state measurement on a chip," *Phys. Rev. Lett.* **105**(20), 200503 (2010).
37. R. Trebino, *Frequency-Resolved Optical Gating: The measurement of Ultrashort Laser Pulses*, (Springer Science & Business Media, 2012).
38. S. M. Eaton, H. Zhang, M. L. Ng, J. Li, W. J. Chen, S. Ho, and P. R. Herman, "Transition from thermal diffusion to heat accumulation in high repetition rate femtosecond laser writing of buried optical waveguides," *Opt. Express* **16**(13), 9443–9458 (2008).
39. S. Eaton, H. Zhang, P. Herman, F. Yoshino, L. Shah, J. Bovatsek, and A. Arai, "Heat accumulation effects in femtosecond laser-written waveguides with variable repetition rate," *Opt. Express* **13**(12), 4708–4716 (2005).
40. W. P. Huang and C. L. Xu, "Simulation of three-dimensional optical waveguides by a full-vector beam propagation method," *IEEE J. Quantum Electron.* **29**, 2639–2649 (1993).
41. T. T. Fernandez, M. Hernandez, B. Sotillo, S. M. Eaton, G. Jose, R. Osellame, A. Jha, P. Fernandez, and J. Solis, "Role of ion migrations in ultrafast laser written tellurite glass waveguides," *Opt. Express* **22**(12), 15298–15304 (2014).
42. A. Yariv, "Coupled-mode theory for guided-wave optics," *IEEE J. Quantum Electron.* **9**, 919–933 (1973).
43. W. J. Chen, S. M. Eaton, H. Zhang, and P. R. Herman, "Broadband directional couplers fabricated in bulk glass with high repetition rate femtosecond laser pulses," *Opt. Express* **16**(15), 11470–11480 (2008).
44. S. M. Eaton, W. Chen, L. Zhang, H. Zhang, R. Iyer, J. S. Aitchison, and P. R. Herman, "Telecom-band directional coupler written with femtosecond fiber laser," *IEEE Photonics Technol. Lett.* **18**, 2174–2176 (2006).

1. Introduction

More than 2000 NP complete problems (non-deterministic polynomial time complete problems) are present in our daily lives [1]. Examples include the clique problem, which requires finding the largest subset of people who all know each other in a social network [2], or the travelling salesman problem that looks for the shortest possible route that visits each city on a map exactly once [3]. The time complexity of an algorithm defines the amount of time that the algorithm takes to be run and is a function of the input problem size. NP complete problems require exponential time complexity functions (exponential solving times) since no polynomial-time algorithms are known for solving them on a non-deterministic Turing machine [4]. Typically, a combinatorial graph problem with N nodes requires an execution time of 2^N times the clock time when solved through brute-force computing. For this particular time complexity function and a typical clock speed of 3.6 GHz of an electronic computer, a graph containing 10 nodes would require ~300 nanoseconds to be solved, while it would take up to 10 years to obtain the exact solution of a graph with 60 nodes.

Scientists and mathematicians continue to seek more efficient methods for solving time demanding problems in reduced execution times. In the past few decades, some alternative approaches to conventional combinatorics for a faster solution of NP complete problems have been proposed, such as the use of soap bubbles [5], three dimensional microfluidic networks [6], protein folding [7–10], quantum [11–15] and DNA computing [16–19]. Optical computing has also been explored in different modalities like beam masking [3], free-space white light interference [20], time delay networks [21–23] and cognitive photonics [22, 24–28]. Unfortunately, all these approaches demand an exponentially increasing amount of physical resources as the problem size increases.

With the new advances in nanofabrication [29] and silicon photonics [30, 31], a new interest in scalable photonic chips capable of solving hard computational problems has resurged in the last few years. Time delay networks are a particularly interesting approach due to their scalability in integrated photonic platforms. Within this modality, optical oracles that solve the Hamiltonian path problem have been proposed [23] and demonstrated [22]. The potential of the optical computing scheme allows speeding up execution times by parallel processing. One of the weaknesses of this approach, however, is the exponential increase of the physical network size with number of nodes. For instance, in the case of the optical oracle for the Hamiltonian path problem, the assignment of suitable delays for each node in the graph is essential to avoid crossover of the optical signals within the network. For the general case of a graph with N nodes and arbitrary connections among different nodes, the optical delays between the nodes of the Hamiltonian path must satisfy the following relation:

$$\sum_{j=1}^N C_j T_j = \sum_{j=1}^N T_j \Leftrightarrow C_1 = C_2 = \dots = C_N = 1, \text{ where } C_j \text{ is a non-negative integer representing how}$$

many times node j has been visited, and N is the total number of nodes in the graph. A possible delay assignment is: $T_j = \Delta t(2^N - 2^{j-1})$ with $j = 1, 2, \dots, N$ and Δt being the pulse width of the injected pulse. This formula was first proposed by Oltean in [23] and was shown to generate a minimal set of optical delays (where the longest delay of the set is the smallest possible). It thus provides an efficient way to construct the network without knowing a priori whether the Hamiltonian path exists. This formula has already proved its validity in the solution of NP complete problems in the context of optical fiber networks [22] and DNA computers [32].

In a previous proof-of-concept demonstration, an optical fiber oracle was employed to find the existence of the Hamiltonian path within a graph by determining the time delay of propagating optical pulses [22]. For a 5-node graph, nanosecond optical pulses were used, and the longest optical fiber length was 1.3 meters. Inspired by this work, here we explore a new pathway to integration and prove down-scaling of the optical oracle network to centimeter spatial dimensions and, correspondingly, femtosecond optical pulse domain. In our approach,

we implement a Hamiltonian path solution of the travelling salesman problem in a compact optical oracle chip by direct laser writing of a coupled optical waveguide network in a borosilicate glass substrate. The Hamiltonian path oracle is interrogated optically, by injecting laser pulses into the waveguide network that maps the topology of a graph with four nodes (or towns). We then measure the time delay between the output pulses from the laser-written photonic circuit. If the Hamiltonian path exists, its delay equals the sum of the travel times needed to visit all nodes of the network, which is made unique by design. Moving from meters of optical fibers [22] towards the millimeter length scale, ultrashort laser pulses in the femtosecond time domain are required when interrogating the laser-written optical oracle. With this decrease in the physical device size and the reduction of the optical pulse width, shorter execution times of the NP computational problems are possible. This first demonstration of a laser-written optical oracle on a robust integrated optics platform proves the potential for reducing the solving time of computationally hard combinatorial problems exploiting the parallelism of light propagation in downscaled optical networks. Thanks to the 3D writing capability of our fabrication technique, further scaling of the network complexity is possible by expanding the graph along the third dimension [33], which would allow new designs with larger number of nodes and compactness.

2. Oracle chip design

The topology of the laser-written optical oracle is shown in Fig. 1. The photonic chip models the Hamiltonian path problem via a unidirectional graph containing four cascaded 2×2 directional couplers, where each coupler plays the role of a node (town), also acting as a beam splitter to direct the light to other nodes. The various nodes are connected to each other by waveguides. In this network, if we consider the central waveguide as input/output ports, then there are three possible paths that can be traveled by a single injected optical pulse: path *A* ($d_{\text{input}} \rightarrow \text{Node 1} \rightarrow d_{12} \rightarrow \text{Node 2} \rightarrow d_{23} \rightarrow \text{Node 3} \rightarrow d_{34} \rightarrow \text{Node 4} \rightarrow d_{\text{output}}$), path *B* ($d_{\text{input}} \rightarrow \text{Node 1} \rightarrow d_{13} \rightarrow \text{Node 3} \rightarrow d_{34} \rightarrow \text{Node 4} \rightarrow d_{\text{output}}$) and path *C* ($d_{\text{input}} \rightarrow \text{Node 1} \rightarrow d_{12} \rightarrow \text{Node 2} \rightarrow d_{24} \rightarrow \text{Node 4} \rightarrow d_{\text{output}}$). To ensure unambiguous pulses arriving from the three possible optical paths, a suitable delay selection for each node was performed corresponding to path lengths of 99.5 mm, 100.9 mm and 102.3 mm for paths *A*, *B* and *C*, respectively.

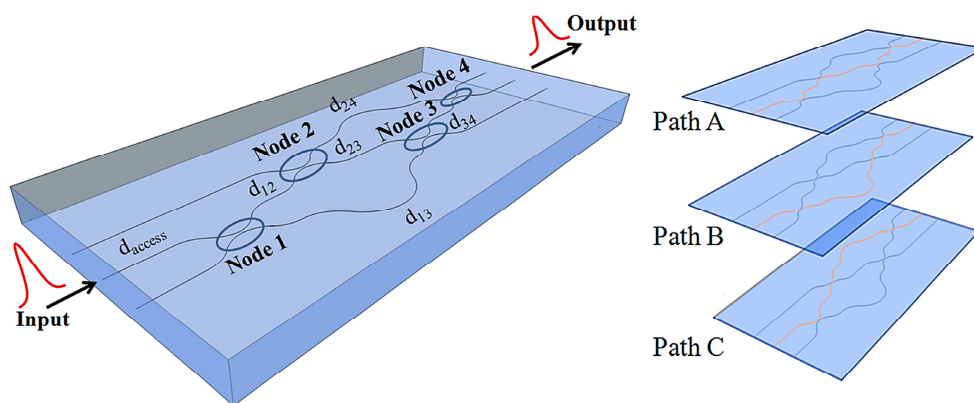


Fig. 1. Femtosecond laser-written optical oracle design. The photonic waveguide network mimics the topology of a network with four nodes or towns in which each town is a 3-dB directional coupler for a 50:50 power splitting ratio.

Table 1 shows a summary of the various segment lengths that make up each of the three paths in the optical oracle. Each node (3-dB directional coupler) has path length of 9.52 mm and $d_{\text{input/output}}$ paths are 0.3 mm long. Assuming a refractive index of 1.5 [31], the first optical pulse (pulse A) is expected to have an arrival time of 165.8 ps relative to propagation in free

space. Under the same assumption, the expected arrival times for pulses B and C are 172.8 ps and 179.6 ps, respectively. Related to downscaling and integration of the optical network, ultrashort optical pulses with pulse durations below ~ 6 ps are required for the resolution of the problem since the minimum time delay for paths B and C is 6.8 ps.

Table 1. Waveguide path lengths designed for the oracle chip.

| | d_{12} (mm) | d_{13} (mm) | d_{23} (mm) | d_{24} (mm) | d_{34} (mm) | Total time (ps) |
|--------|---------------|---------------|---------------|---------------|---------------|-----------------|
| Path A | 0.2 | - | 47.0 | - | 13.6 | 165.8 |
| Path B | - | 58.1 | - | - | 13.6 | 172.8 |
| Path C | 0.2 | - | - | 72.9 | - | 179.6 |

The photonic chip was fabricated in a $100 \times 100 \times 1$ mm³ borosilicate glass (EAGLE2000, Corning) substrate by using femtosecond laser writing. EAGLE2000 glass was previously shown to enable low propagation losses in the near infrared from 800 nm to 1550 nm wavelength [34, 35]. The parameters chosen for the directional couplers coincide with a power splitting ratio of 50% at the output of each arm. Every directional coupler of the oracle chip was fabricated with an S-bend geometry of 40 mm radius of curvature and a separation distance between the two nearby waveguides of 7 μ m with a length of 700 μ m each. Results after a proper characterization reported waveguides with nearly circular single modes of 6.5 μ m \times 7.1 μ m as a MFD when guiding light at 800 nm wavelength, which is similar to the MFD for waveguides written in EAGLE2000 by other groups [35, 36]. The waveguides presented a propagation loss of 0.9 dB/cm and a total insertion loss for the entire oracle chip of 10.6 dB (considering 0.4 dB coupling loss/facet and 1.39 dB bend loss in the directional couplers). See Appendix for further fabrication details.

3. Characterization of the optical oracle

Since time delays between consecutive optical pulses within the oracle chip are ~ 6 ps, the optical problem can be resolved for input pulse widths shorter than this value. The use of ultrashort pulses, requires an ultrafast optical technique for the detection of the output pulses travelling through the oracle. An optical cross-correlation technique [37] was used to study the pulse distribution in time from the optical oracle by using an 800-nm wavelength Ti:Sapphire femtosecond oscillator having ~ 200 fs pulse width (FWHM), 1 nJ pulse energy and 80 MHz repetition rate. The output of the laser was split into two separate beam paths as shown in Fig. 2(a).

For the signal arm, 70% of the power from the original laser beam was coupled into optical oracle chip using a 0.16-NA microscope objective. A 0.25-NA lens was used to collect light at the output of the oracle. Optical spectra collected before and after the optical oracle confirms there is no noticeable self-phase modulation of the ultrashort pulses along the waveguides, which have a peak intensity of 10 GW/cm² when coupled to the oracle.

The remaining 30% of the light goes to the reference arm which is optically delayed via a motorized linear stage with an accuracy of 2 μ m. After this, the two beams are non-collinearly focused by a $f = 75$ mm plano-convex lens onto a 2 mm length BBO crystal cut at an angle of 30°. A SCHOTT BG39 color glass filter is used for blocking the fundamental beams at 800-nm wavelength while an iris is used to remove the steady-state second harmonic signals. The resulting second harmonic cross-correlated signal is collected by a silicon photodiode detector, connected to a lock-in amplifier to discriminate the signal from the noise.

The optical cross-correlation setup was used to study two different oracle samples, a complete one (containing the Hamiltonian path), and a control sample in which the Hamiltonian path was intentionally broken with a 20 μ m gap inserted along the waveguide d_{23} . Results obtained from optical cross-correlation measurements for both cases are shown in Fig. 2(b) and Fig. 2(c). Absolute time zero was defined by the autocorrelation signal detected in free space, that is when the chip is removed from the correlation setup (top graph in Fig. 2(b)). As shown in Fig. 2(b), the time between the generated autocorrelation signal and the

first output pulse from the optical chip is 163 ps, in good agreement with expected theoretical value of 165.8 ps (Table 1). This time delay is equivalent to a distance of 24.45 mm, corresponding to the total optical path length of path *A*.

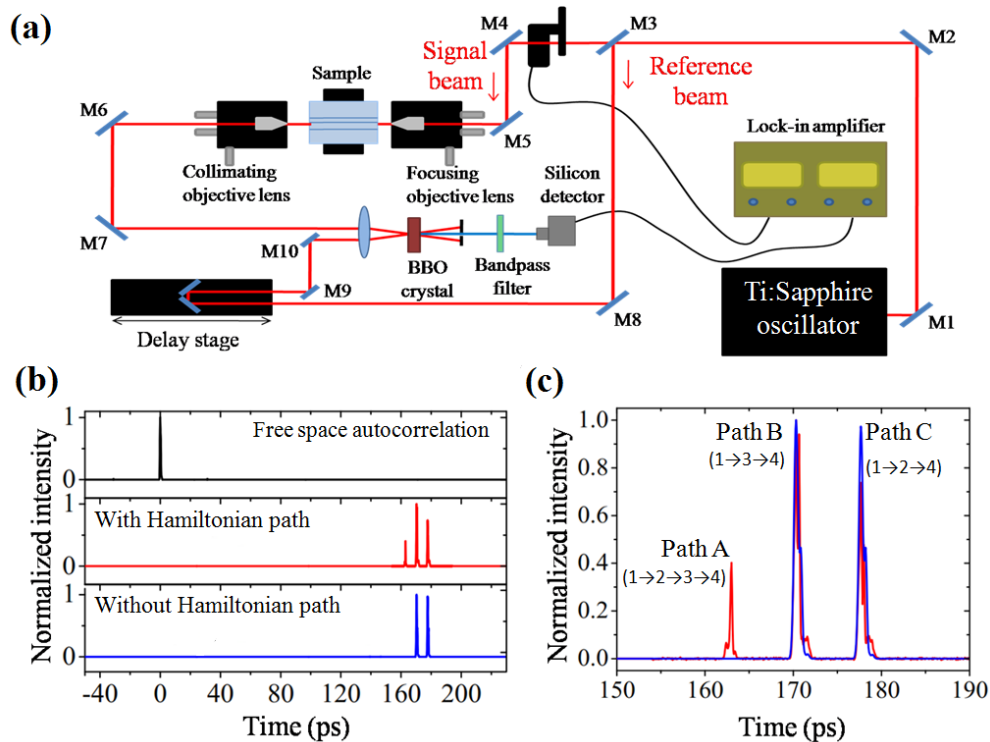


Fig. 2. (a) Optical cross-correlator setup for time resolved measurements. (b) Optical autocorrelation measured in free space, and after propagation in the oracle chip and in the control sample, respectively. (c) Femtosecond output pulses in time domain detected from oracle chip and control sample. The node number visited by each pulse is indicated next to every peak.

From the cross-correlation measurements of the oracle chip, three output peaks are detected (red curves in Fig. 2(b) and Fig. 2(c)), with absolute time delays $|\Delta t_{A \rightarrow B}| = 7.3$ ps, $|\Delta t_{B \rightarrow C}| = 7.3$ ps and $|\Delta t_{A \rightarrow C}| = 14.7$ ps. The output pulse arrival times are 163 ps, 170.3 ps and 177.7 ps for peaks *A*, *B* and *C*, respectively. These experimentally measured arrival times are in excellent agreement with the theoretical design values (Table 1). The time of arrival of 163 ps corresponds, by design, to the Hamiltonian path travelled by pulse *A*, in which all the nodes in the graph are visited exactly once.

From the cross-correlation of the control sample (blue curves in Fig. 2(b) and Fig. 2(c)), peak *A* disappears indicating the absence of the Hamiltonian path. Peaks *B* and *C* are present since paths *B* and *C* still are inscribed into the encoding scheme.

4. Summary

In summary, we have realized the first integrated laser-written optical oracle based on time delay networks for the solution of the Hamiltonian path problem. Direct laser writing technique is a promising tool for the implementation of different NP computational problems into compact glass substrates as optical analog devices. Inscription of specific graph schemes through this fabrication method enables integration and scalability of the optical network in comparison with graphs based on optical fiber connections. Future designs could exploit 3D patterning and parallel processing, advantages of femtosecond laser writing, to further

enhance integration. Based on the waveguide parameters achieved in this work, a 20-node graph may be inscribed into a $100 \times 100 \times 1$ mm³ glass substrate by exploiting parallelism of the optical network and its third dimension (depth) during fabrication. To enhance compactness, two graph layers, containing 10 nodes each, could be connected to each other by a curved optical waveguide that inverts the direction of light propagation for the second layer. The use of ultrafast optical techniques would be a necessity for the detection of the optical signals in this type of device due to the miniaturization of the networks. Assuming single point detection at the output of the network, this oracle's decision time, limited only by parallel pulse propagation time within the network, would require ~ 1 ns in comparison with the ~ 6 μ s needed for an electronic computer to find the combinatorial solution considering only two-directional nodes and a clock speed of 3.6 GHz.

5. Appendix

5.1 Optical waveguide fabrication

The laser used for waveguide fabrication was a regeneratively amplified Yb:KGW system (Pharos, Light Conversion) with 230 fs pulse duration and 1030 nm wavelength. Computer-controlled, 3-axis motion stages (ABL-1000, Aerotech) interfaced by CAD-based software (ScaBase, Altechna) with an integrated acousto-optic modulator (AOM) were used to translate the sample relative to the laser to form the desired photonic structures. After a careful optimization procedure similar to that described in [38], we found that the best laser processing parameters for achieving low-loss waveguides at 800 nm characterization wavelength were a 0.42 NA focusing objective, 1 MHz repetition rate, 450 nJ pulse energy and a scan speed of 50 mm/s.

The morphology of laser-inscribed waveguides was characterized using white-light optical microscopy in transmission mode (Eclipse ME600, Nikon), revealing the typical core-cladding structure (Fig. 3(a), (b)) for buried structures fabricated in borosilicate glass at high repetition rates [39]. For waveguide transmission measurements, high resolution 3-axis manual positioners (Nanomax MAX313D, Thorlabs) were used. The four-axis central waveguide manipulator (MicroBlock MBT401D, Thorlabs) enabled longer travel transverse displacement. A laser diode at 808 nm wavelength (S1FC808, Thorlabs) was coupled to the waveguides using a single-mode fiber (780HP, Thorlabs). At the waveguide output, light was coupled to an optical power meter (818-SL, Newport) to measure the power transmitted through the waveguide. To capture the near-field waveguide mode profile, a $60\times$ asphere (5721-H-B, Newport) was used to image the light to a beam profiler (SP620U, Spiricon).

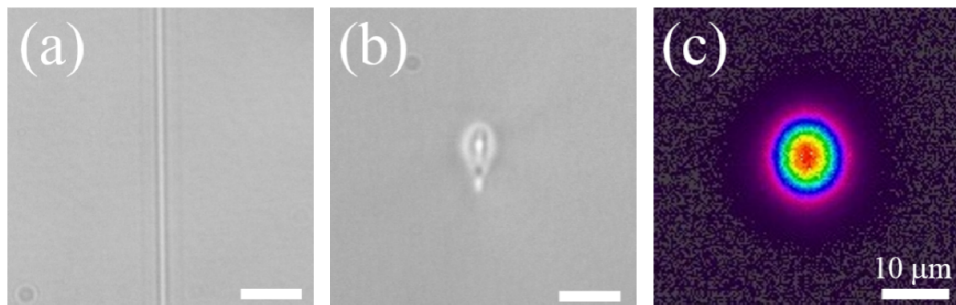


Fig. 3. Waveguide characterization. (a) Overhead white-light microscopy of a waveguide. Two different zones can be clearly differentiated: the core along the central part, where maximum change in refractive index is reached, and the cladding at its surrounding. (b) Cross-sectional white-light-microscopic image of the waveguide at its end facet. (c) Guided mode at 808 nm wavelength with MFD of $6.5 \mu\text{m} \times 7.1 \mu\text{m}$.

Nearly circular single mode waveguides with a MFD of $6.5 \mu\text{m} \times 7.1 \mu\text{m}$ (Fig. 3(c)) were observed at 800 nm wavelength, which is similar to the MFD for waveguides written in EAGLE2000 by other groups [35, 36]. The waveguide propagation loss was 0.9 dB/cm and the total insertion loss for oracle chip was 10.6 dB (including 0.4 dB coupling loss/facet and 1.39 dB bend loss in the directional couplers).

5.2 Directional coupler fabrication

Optical directional couplers with S-bend geometries (Fig. 4(a)) were fabricated over a wide range of parameters to determine the optimum bend radius R , separation distance s and interaction length L for the oracle chip in Fig. 1. We first studied the bend loss as a function of bend radius. Here we define the bend loss as the additional insertion loss in a single arm of a double S-bend waveguide compared to a straight waveguide. This loss therefore includes pure bend loss from the four arcs and transition loss from the six points where there is an abrupt change in curvature. From Fig. 4(b), we found a reasonable trade-off between bend loss and device size for a radius of curvature of 40 mm. In Fig. 4(b), we also show a comparison with a theoretical simulation performed with RSoft BeamPROP beam propagation method (BPM) [40] with a circular step refractive index profile. We selected the diameter to be $2.5 \mu\text{m}$ to match the core diameter in the microscope image in Fig. 3(a) and chose a refractive index contrast of $\Delta n = 4.5 \times 10^{-3}$ as it resulted in a simulated MFD of $\sim 7 \mu\text{m}$, equal to the experimental value. The small discrepancy between the theoretical and experimental bend loss in Fig. 4(b) is attributed to the simplified assumption of a step index profile, as the actual refractive index profile is more complex, as shown in Fig. 3(b) and also reported elsewhere [38, 41].

For a bend radius of 40 mm, we then selected the optimum separation distance, s , between the two nearby waveguides in a single directional coupler. Experimental characterization (Fig. 4(c)) shows that the beat length (l_B), the length necessary for a full power oscillation, increases with waveguide separation since the coupling coefficient falls off exponentially with increasing distance. The discrepancy between simulated and experimental data at $s = 10 \mu\text{m}$ is attributed once again to the step index profile assumed in the simulation. We selected a separation distance of $7 \mu\text{m}$ for the directional coupler building block to minimize the interaction length needed for 3-dB coupling. We could not exploit shorter separation distances because below $s = 6 \mu\text{m}$, we found that directional couplers were more sensitive to fabrication fluctuations. At $s = 7 \mu\text{m}$, the power coupling ratio (CR), defined as the normalized power in the cross port waveguide, varies sinusoidally between 0 and 1, as predicted by coupled mode theory [42, 43]. An interaction length of $700 \mu\text{m}$ for a 50:50 power splitting ratio was selected after fitting the experimental values to a sine square function (Fig. 4(d)) [44].

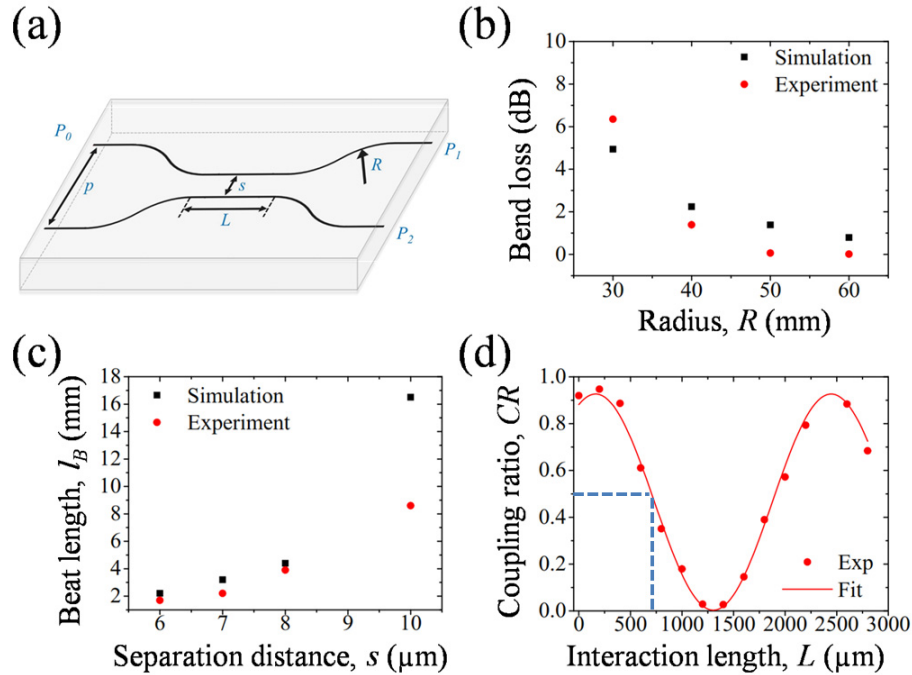


Fig. 4. (a) Directional coupler with S-bend geometry. The different parameters are: pitch between access ports, p , radius of curvature, R , separation distance, s , and interaction length, L . P_0 represents the optical input power injected into a single arm while P_1 and P_2 are the through and cross output port powers, respectively. (b) Experimental and simulated bend loss as a function of bend radius for a S-bend waveguide. (c) Beat length as a function of the separation distance. (d) Experimental power coupling ratio versus interaction length for a separation distance of $s = 7 \mu\text{m}$. The dot lines in blue indicate a 50% power coupling ratio at an interaction length of $700 \mu\text{m}$.

Funding

Singapore Ministry of Education (MOE2011-T3-1-005); DIAMANTE MIUR-SIR Grant; FemtoDiamante Cariplo ERC Reinforcement Grant.

Acknowledgments

We are grateful to Luigino Criante for access to the FemtoFab facility at CNST-IIT Milano for the laser fabrication experiments. We are also grateful to Stefano Longhi and Giuseppe Della Valle for valuable scientific discussions.